Inorganica Chimica Acta 384 (2012) 225–232

Contents lists available at SciVerse ScienceDirect

Inorganica Chimica Acta

journal homepage: www.elsevier.com/locate/ica

A series of [Cu(N–N)(P–P)]BF_4 complexes: Luminescence quenching caused by electron-configuration transformation in excited state

Liming Zhang [a], Shumei Yue [b], Bin Li [a,*], Di Fan [a]

[a] State Key Laboratory of Luminescence and Applications, Changchun Institute of Optics Fine Mechanics and Physics, Chinese Academy of Sciences, Changchun 130033, PR China
[b] College of Chemistry, Changchun Normal University, Changchun 130032, PR China

ARTICLE INFO

Article history:
Received 20 July 2009
Received in revised form 29 November 2011
Accepted 2 December 2011
Available online 9 December 2011

Keywords:
Cu(I) complex
Excited state
Luminescence quenching
Electron-configuration

ABSTRACT

In this paper, we report a series of [Cu(N–N)(P–P)]BF_4 complexes based on two phosphorous ligands and three 1,10-phenanthrolin derived diimine ligands, including their syntheses, characterizations, crystal structures. Their photophysical properties were experimentally measured and theoretically analyzed by time-dependent density functional theory (TD-DFT). It is found that the introduction of too many fused phenyl rings into diimine ligand leads to luminescence absence of corresponding [Cu(N–N)(P–P)]$^+$ complexes at room temperature. A detailed analysis suggests that the thermal activated electron-configuration transformation between the [Cu(N–N)(P–P)]$^+$ triplet metal-to-ligand-charge-transfer (^{3}MLCT) state and the lowest lying excited state of its diimine ligand (^{3}LC) is responsible for the luminescence quenching.

1. Introduction

The development of practical components for chemical sensors, display devices, probes of biological systems, and solar energy conversion schemes has sparked an interest in complexes of diimine ligands with transition metals, especially heavy metal ions such as ruthenium(II) and rhenium(I) [1–9]. At the same time, the strong appeal of using cheaper copper complexes to replace more expensive compounds based on noble metal ions and the need for a deeper understanding of correlation between structural processes and photophysical properties have led to continuous progress in the design of photoluminescent Cu(I) complexes. However, the emission signal from the charge-transfer (CT) excited state of Cu(I) complexes is typically weak and short-lived because the lowest-energy CT state of a d^{10} system involves excitation from a metal–ligand dσ^* orbital [10–12]. An important consequence is that the excited state typically prefers tetragonally flattened geometry, whereas the ground state usually adopts a more tetrahedral-like coordination geometry that is appropriate for a closed-shell ion. Aside from reducing the energy content, the geometry relaxation that occurs in the excited state facilitates relaxation back to the ground state [13–15]. Moreover, donor media also tend to quench the excited state. McMillin first reported this type of exciplex quenching, and by now, many other studies have confirmed the mechanism.

Mixed-ligand systems involving triphenylphosphane looked promising because they exhibited long excited state lifetimes in solid state and frozen solution [16–19]. A series of new mixed-ligand copper(I) polypyridine and phenanthroline complexes such as [Cu(N–N)(POP)]$^+$ [POP = bis(2-(diphenylphosphanyl)phenyl) ether], which are superior emitters, have been synthesized. It is found that solvent-induced exciplex quenching is relatively inefficient for the CT excited state of this POP system. In addition, introduction of sterically blocking ligands can impede geometric relaxation as well as solvent attack. Here, steric effects cooperate to effectively block the excited state close to the ground-state geometry, which has been proved by the theoretical studies finished by Feng and coworkers on [Cu(N–N)(P–P)]$^+$ system [20]. For a typical phosphorescent Cu(I) complex, the two highest occupied molecular orbitals (HOMOs) have predominant metal Cu d character, while, the two lowest unoccupied orbitals (LUMOs) are essentially π^* orbitals localized on the diimine ligand. The photoluminescence corresponds to the lowest triplet T_1 and is thus assigned as a character of metal-to-ligand-charge-transfer ^{3}MLCT [d(Cu) → π^*(diimine ligand)]. The MLCT excited states of cuprous diimine compounds are often luminescent and play important roles in photoinduced electron and energy transfer process.

In this paper, however, we report another potential quenching mechanism leading to ^{3}MLCT luminescence absence. Based on photophysical properties obtained from a series of [Cu(N–N)(P–P)]BF_4 complexes, it is found that the introduction of too many fused phenyl rings into diimine ligand compromises ^{3}MLCT luminescence. Systematical research suggests that the electron-configuration transformation between ^{3}MLCT state and triplet state of

* Corresponding author. Tel./fax: +86 431 86176935.
E-mail address: lib020@yahoo.cn (B. Li).

0020-1693/$ - see front matter © 2011 Elsevier B.V. All rights reserved.
doi:10.1016/j.ica.2011.12.002

diimine ligand in excited state [Cu(N–N)(P–P)]BF_4 is responsible for the luminescence quenching.

2. Experimental

Scheme 1 shows the molecular structures of ligands and their corresponding Cu(I) complexes.

Bis[2-(diphenylphosphino)phenyl] ether (referred as POP), triphenylphosphine (referred as PPh_3), 1,10-phenanthroline (referred as phen), ethane-1,2-diamine, benzene-1,2-diamine, naphthalene-2,3-diamine were purchased from Aldrich Chemical Co. and used without further purification.

2.1. Synthesis of ligands

1,10-Phenanthroline-5,6-dione was synthesized according to the literature procedure [21].

A typical synthesis procedure for 1,4,8,9-tetraaza-triphenylene (referred as Pyphen), 4,5,9,14-tetraaza-benzo[b]triphenylene (referred as DPPZ) and 4,5,9,16-tetraaza-dibenzo[a,c]naphthacene (referred as BDPZ) is described as follows: a mixture of 5 mmol of 1,10-phenanthroline-5,6-dione, 5.5 mmol of diamine, 25 mL of ethanol and 0.05 mmol of 4-methylbenzenesulfonic acid was heated under 80 °C for 10 h, the crude product was filtered and then recrystallized from ethanol to give the pure desired product.

Pyphen: colorless crystal. ^{1}H NMR (300 Hz, $CDCl_3$, 25 °C): δ 9.51 (d, 2 H, J = 8.0 Hz),9.31 (d, 2 H, J = 8.0 Hz), 9.01 (s, 2 H), 7.82 (m, 2 H). *Anal.* Calc. for $C_{14}H_8N_4$: C, 72.41; H, 3.45; N, 24.14. Found: C, 72.24; H, 3.48; N, 23.98%.

DPPZ: light brown crystal. ^{1}H NMR (300 Hz, $CDCl_3$, 25 °C): δ 9.65 (d, 2H, J = 8.0 Hz), 9.27 (d, 2H, J = 8.0 Hz), 8.35 (d, 2H, J = 6.4 Hz), 7.91 (d, 2H, J = 6.4 Hz), 7.80 (m, 2H). *Anal.* Calc. for $C_{18}H_{10}N_4$: C, 76.60; H, 3.55; N, 19.86. Found: C, 75.95; H, 3.61; N, 19.81%.

BDPZ: brown crystal. ^{1}H NMR (300 Hz, $CDCl_3$, 25 °C): δ 9.69 (d, 2H, J = 8.0 Hz), 9.28 (d, 2H, J = 8.0 Hz), 8.99 (s, 2H), 8.23 (d, 2H, J = 8.0 Hz), 7.82 (m, 2H), 7.65 (d, 2H, J = 8.0 Hz). *Anal.* Calc. for $C_{22}H_{12}N_4$: C, 79.52; H, 3.61; N, 16.87. Found: C, 79.30; H, 3.74; N, 16.79%.

2.2. Synthesis of [Cu(N–N)(P–P)]BF_4

All the Cu(I) complexes were synthesized according to the well-known literature procedure [22]. Their identities were confirmed by NMR, elemental analysis, and single crystal XRD (see Supporting information).

[Cu(Pyphen)(PPh_3)$_2$]BF_4: ^{1}H NMR (300 Hz, $CDCl_3$, 25 °C): δ 9.50 (d, 2 H, J = 8.0 Hz), 9.32 (d, 2 H, J = 8.0 Hz), 8.99 (s, 2 H), 8.01–7.78 (m, 20 H), 7.51–7.46 (m, 12 H). ^{31}P NMR δ +1.71 (s). *Anal.* Calc. for $C_{50}H_{38}BCuF_4N_4P_2$: C, 66.20; H, 4.22; N, 6.18. Found: C, 66.23; H, 4.28; N, 6.09%.

[Cu(DPPZ)(PPh_3)$_2$]BF_4: 1H NMR (300 Hz, $CDCl_3$, 25 °C): δ 9.64 (d, 2H, J = 8.0 Hz), 9.26 (d, 2H, J = 8.0 Hz), 8.31 (d, 2H, J = 6.4 Hz), 7.99–7.79 (m, 22H), 7.48–7.41 (m, 12 H). ^{31}P NMR δ + 1.69 (s). *Anal.* Calc. for $C_{54}H_{40}BCuF_4N_4P_2$: C, 67.76; H, 4.21; N, 5.85. Found: C, 67.68; H, 4.27; N, 5.93%.

[Cu(BDPZ)(PPh_3)$_2$]BF_4: ^{1}H NMR (300 Hz, $CDCl_3$, 25 °C): δ 9.70 (d, 2H, J = 8.0 Hz), 9.27 (d, 2H, J = 8.0 Hz), 8.98 (s, 2H), 8.21 (d, 2H, J = 8.0 Hz), 7.98–7.80 (m, 20H), 7.61 (d, 2H, J = 8.0 Hz), 7.49–7.40

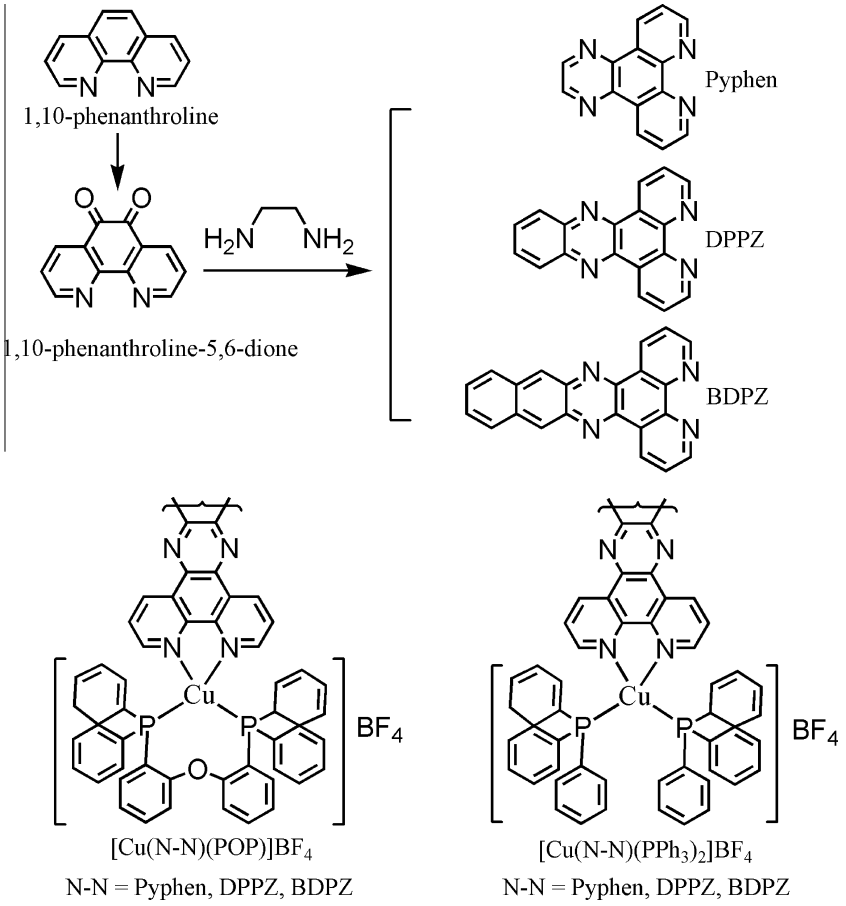

Scheme 1. Synthetic procedure of ligands and molecular structures of Cu(I) complexes.

(m, 12H). ^{31}P NMR δ +1.70 (s). *Anal.* Calc. for $C_{58}H_{42}BCuF_4N_4P_2$: C, 69.16; H, 4.20; N, 5.56. Found: C, 69.27; H, 4.28; N, 5.43%.

[Cu(Pyphen)(POP)]BF$_4$: ^{1}H NMR (300 Hz, $CDCl_3$, 25 °C): δ 9.50 (d, 2 H, J = 8.0 Hz), 9.28 (d, 2 H, J = 8.0 Hz), 9.00 (s, 2 H), 7.88–7.76 (m, 20 H), 7.37–7.33 (m, 10H). ^{31}P NMR δ +1.65 (s). *Anal.* Calc. for $C_{50}H_{36}BCuF_4N_4OP_2$: C, 65.19; H, 3.94; N, 6.08. Found: C, 65.11; H, 4.01; N, 6.17%.

[Cu(DPPZ)(POP)]BF$_4$: ^{1}H NMR (300 Hz, $CDCl_3$, 25 °C): δ 9.63 (d, 2H, J = 8.0 Hz), 9.28 (d, 2H, J = 8.0 Hz), 8.32 (d, 2H, J = 6.4 Hz), 7.91–7.78 (m, 22H), 7.35–7.30 (m, 10H). ^{31}P NMR δ +1.66 (s). *Anal.* Calc. for $C_{54}H_{38}BCuF_4N_4OP_2$: C, 66.78; H, 3.94; N, 5.77. Found: C, 66.71; H, 3.78; N, 5.84%.

[Cu(BDPZ)(POP)]BF$_4$: ^{1}H NMR (300 Hz, $CDCl_3$, 25 °C): δ 9.68 (d, 2H, J = 8.0 Hz), 9.25 (d, 2H, J = 8.0 Hz), 8.97 (s, 2H), 8.20 (d, 2H, J = 8.0 Hz), 7.89–7.77 (m, 22H), 7.36–7.30 (m, 10H). ^{31}P NMR δ +1.63 (s). *Anal.* Calc. for $C_{58}H_{40}BCuF_4N_4OP_2$: C, 68.21; H, 3.95; N, 5.49. Found: C, 68.40; H, 3.84; N, 5.56%.

2.3. Computational methods and measurements

DFT calculations were performed on the three diimine ligands, Pyphen, DPPZ and BDPZ, using RB3LYP/6-31G(d). Singlet excitation calculations on [Cu(N–N)(PPh_3)$_2$]BF_4, where N–N = Pyphen, DPPZ, and BDPZ, were performed by TD-DFT using RB3LYP/SBKJC. The initial geometries were obtained from single crystal data of their corresponding complexes. All the computations were finished by PC GAMESS.

Excited state lifetimes were obtained with a 355 nm light generated from the Third-Harmonic-Generator pumped, which using pulsed Nd:YAG laser as excitation source. The Nd:YAG laser possesses a line width of 1.0 cm^{-1}, pulse duration of 10 ns and repetition frequency of 10 Hz. A Rhodamine 6G dye pumped by the same Nd:YAG laser was used as the frequency-selective excitation source. All the photoluminescence (PL) spectra were measured with a Hitachi F-4500 fluorescence spectrophotometer. UV–Vis absorption spectra were recorded using a Shimadzu UV-3101PC spectrophotometer. ^{1}H and ^{31}P NMR spectra were obtained with the use of a Varian INOVA 300 spectrometer. Elemental analyses were performed on a Carlo Erba 1106 elemental analyzer. Single crystals data were collected on a Siemens P4 single-crystal X-ray diffractometer with a Smart CCD-1000 detector and graphite-monochromated Mo Kα radiation, operating at 50 kV and 30 A at 298 K. All hydrogen atoms were calculated. All measurements were carried out in the air at room temperature without being specified.

3. Results and Discussion

3.1. Geometric structures of [Cu(N–N)(P–P)]BF$_4$ complexes

Crystal structures of [Cu(N–N)(PPh_3)$_2$]BF_4 and [Cu(N–N)(POP)]BF_4, where N–N = Pyphen, DPPZ, and BDPZ, are depicted in Figs. 1a–1f. Geometric parameters summarized in Table 1 suggest that the Cu(I) center in all six complexes has a distorted tetrahedral geometry. The dihedral angles between N–Cu–N and P–Cu–P planes for the six complexes are measured to be 87.43°, 87.91°, 88.72°, 78.54°, 89.58°, and 86.59°, respectively. Cu–N bond lengths of the six Cu(I) complexes localize in a region of 2.05–2.11 Å which are comparable to literature values [20,22]. It is also observed that Cu–N bond lengths in POP system are usually shorter than those in PPh_3 system, indicating a stronger Cu–N bond in POP system. On the other hand, Cu–P bond lengths of the six Cu(I) complexes are similar to each other. The oxygen atom of POP ligand in [Cu(N–N)(POP)]BF_4 complexes localizes at a distance of ~3 Å from the Cu(I) center and opposite to that of coordinated N atoms,

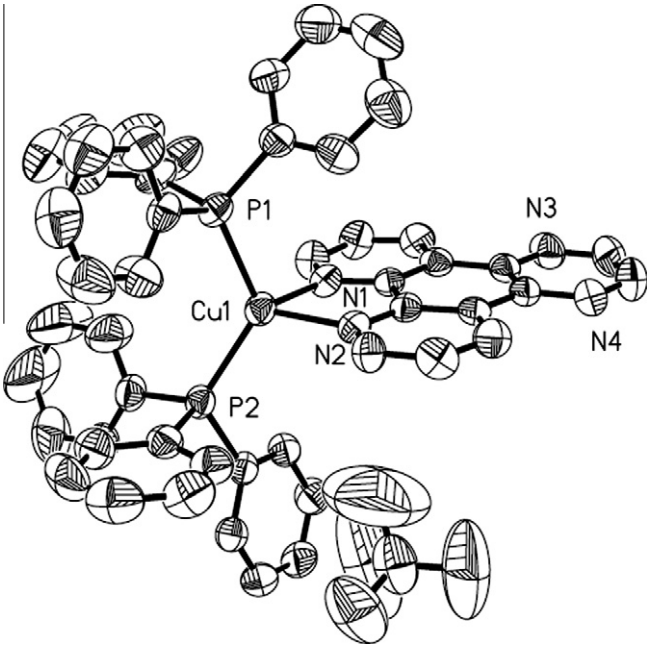

Fig. 1a. Structure of [Cu(Pyphen)(PPh_3)$_2$]BF_4.

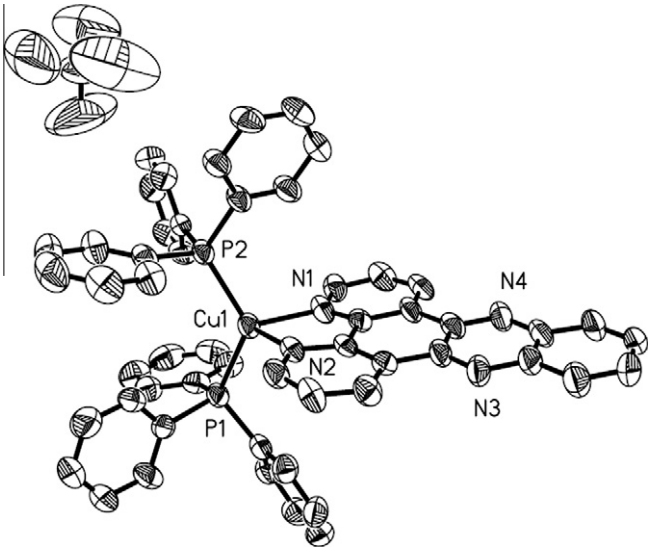

Fig. 1b. Structure of [Cu(DPPZ)(PPh_3)$_2$]BF_4.

indicating a weak interaction between oxygen atom and Cu(I) center. Similar Cu...O separations have also been reported in POP-based Cu(I) complexes that contain 1,10-phenanthroline and derived ligands [20,22].

N–Cu–N bond angles of the Cu(I) complexes, except for [Cu(DPPZ)(POP)]BF_4, are quite similar to each other (~80°) with a little variation. As for [Cu(DPPZ)(POP)]BF_4, the N–Cu–N bond angle is somewhat greater, 81.2°, clearly due to reduced static congestion caused by the large dihedral angle between N–Cu–N and P–Cu–P planes of [Cu(DPPZ)(POP)]BF_4 (89.58°). In contrast, P–Cu–P bond angle varies dramatically from 112.69° for [Cu(BDPZ)(POP)]BF_4 to 124.15° for [Cu(Pyphen) (PPh_3)$_2$]BF_4 as shown in Table 1. Considering POP's natural bite angle of 102.2°, with a flexibility range from 86° to 120°, these large P–Cu–P bond angles in POP-based Cu(I) complexes suggest a crowded coordination environment at Cu(I) center [23].

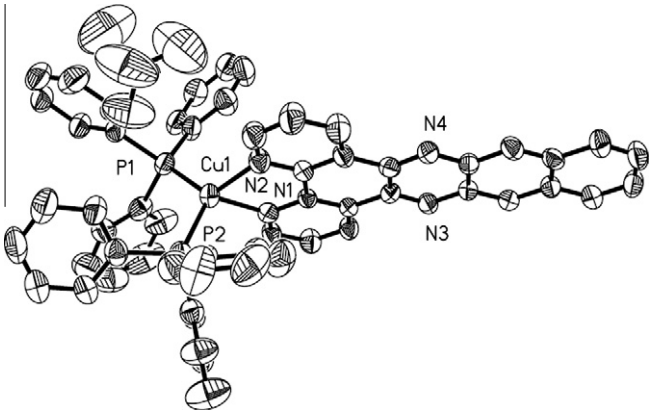

Fig. 1c. Structure of $[Cu(BDPZ)(PPh_3)_2]BF_4$.

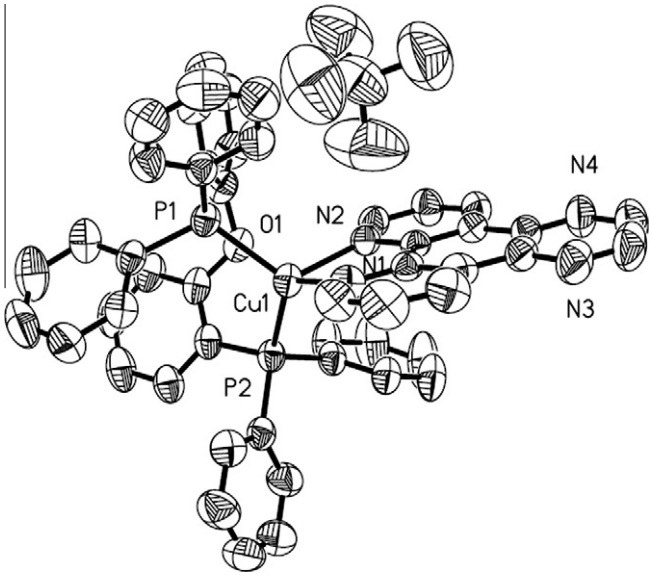

Fig. 1d. Structure of $[Cu(Pyphen)(POP)]BF_4$.

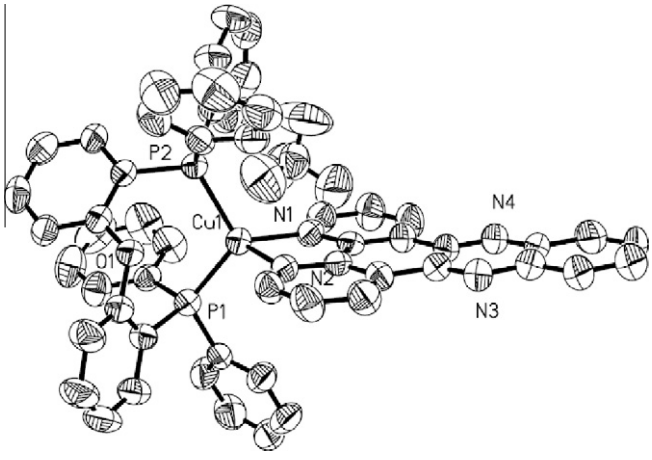

Fig. 1e. Structure of $[Cu(DPPZ)(POP)]BF_4$.

It is also observed that there is inter- and inner-molecular π-stacking within solid state $[Cu(BDPZ)(P–P)]BF_4$ complexes due to BDPZ's large coplanar conjugation plane, where P–P = $(PPh_3)_2$ and POP (see Supporting information for a detailed presentation). As

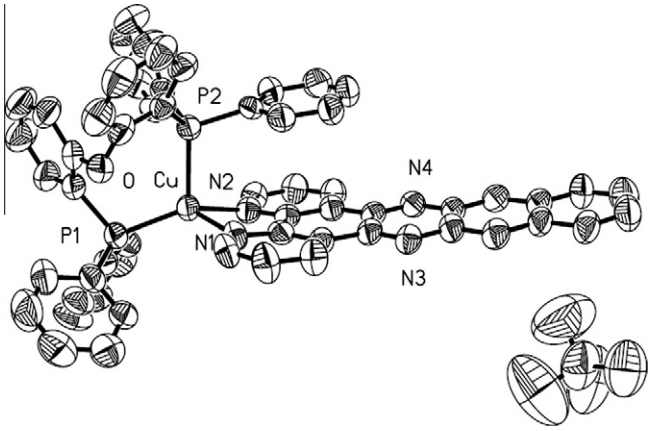

Fig. 1f. Structure of $[Cu(BDPZ)(POP)]BF_4$.

for solid $[Cu(BDPZ)(PPh_3)_2]BF_4$, every two molecules are bonded head-to-head, where BDPZ moiety is defined as the "head", due to π–π attraction between BDPZ rings. The dihedral angle between BDPZ rings is measured to be as small as 3.48° with a distance of 3.399 Å, which confirms that there is face-to-face π–π stacking between the two BDPZ rings. In addition to this kind of inter-molecular π-stacking interaction, it appears that there is additional inner-molecular π-stacking interaction within solid state $[Cu(BDPZ)(POP)]BF_4$, which actually increases π–π attraction and allows $[Cu(BDPZ)(POP)]BF_4$ molecule to take a more organized geometry. Similarly, $[Cu(BDPZ)(POP)]BF_4$ molecules also take the "head-to-head" dual-molecule packing mode, and the two BDPZ rings are aligned parallel to each other with a distance of 3.340 Å. Within one $[Cu(BDPZ)(POP)]BF_4$ molecule, small N(1)–Cu–P(2) and N(2)–Cu–P(2) bond angles allow one of POP's phenyl ring to align almost parallel to BDPZ ring so that their mean planes intersect with an angle of 4.21°, and the approximate distance between POP phenyl ring and BDPZ ring is only 3.243 Å. This pseudo sandwich configuration is believed to be a rigid structure and has been proved to be efficient on suppressing nonradiative decay process of ^{3}MLCT excited state, leading to largely enhanced PL performances [24].

3.2. Electronic absorptions and electronic structures

Fig. 2 shows UV–Vis absorption spectra of $[Cu(N–N)(PPh_3)_2]BF_4$ and $[Cu(N–N)(POP)]BF_4$ in CH_2Cl_2 with a concentration of 1×10^{-5} mol/L, where N–N = Pyphen, DPPZ, and BDPZ. It can be observed that each electronic absorption spectrum is typically composed of a high-energy absorption band ranging from 330 to 250 nm and a low-energy absorption band ranging from 350 to 500 nm. The former one corresponds to ligands $\pi \rightarrow \pi^*$ transitions according to the previous report [25]. While, the latter one is experimentally assigned as MLCT transition absorption. In order to get a further understanding on the electronic transition nature, time dependent density functional theory (TD-DFT), which has been proved to be an excellent tool when exploring molecular excited state properties, was performed on $[Cu(N–N)(PPh_3)_2]BF_4$, where N–N = Pyphen, DPPZ, and BDPZ [20].

As shown in Table 2, their HOMOs have an evident metal Cu character, admixed with large contributions from the phosphorous ligand, while, LUMOs are essentially diimine ligand π^* orbitals (see Supporting information for a graphic presentation). The calculated onset transitions all correspond to electron transition from HOMO to LUMO, and their excitation energies correlate quite well with their experimentally recorded absorption edges (λ_{edg}) shown in Fig. 2. It is thus confirmed that the onset electronic transitions of $[Cu(N–N)(PPh_3)_2]BF_4$ are all MLCT ones. Given $[Cu(N–N)(POP)]BF_4$'s

Table 1
Selected bond lengths (Å) and angles (°).

	[Cu(N–N)(P–P)]BF_4, N–N═, P–P═,					
	Pyphen $(PPh_3)_2$	DPPZ $(PPh_3)_2$	BDPZ $(PPh_3)_2$	Pyphen POP	DPPZ POP	BDPZ POP
Cu(1)–N(1)	2.087(5)	2.105(7)	2.110(7)	2.054(2)	2.051(5)	2.060(4)
Cu(1)–N(2)	2.107(5)	2.069(7)	2.060(7)	2.118(2)	2.063(5)	2.086(4)
Cu(1)–P(1)	2.284(2)	2.272(2)	2.245(3)	2.2425(8)	2.2420(18)	2.2186(16)
Cu(1)–P(2)	2.268(2)	2.275(2)	2.261(3)	2.2633(8)	2.2420(18)	2.3194(15)
Cu...O	N/A[a]	N/A[a]	N/A[a]	2.977	3.079	3.213
N(1)–Cu–N(2)	79.2(2)	79.4(3)	79.9(3)	79.52(9)	81.2(2)	79.99(17)
N(1)–Cu–P(1)	105.22(16)	111.24(18)	104.9(2)	114.32(6)	117.21(15)	123.54(13)
N(2)–Cu–P(1)	108.31(15)	108.63(18)	125.1(2)	116.81(6)	112.83(14)	133.07(13)
N(1)–Cu–P(2)	117.03(16)	111.1(2)	114.7(2)	125.85(6)	116.72(14)	101.59(13)
N(2)–Cu–P(2)	113.87(16)	113.57(18)	106.7(2)	101.76(6)	111.50(14)	98.66(12)
P(1)–Cu–P(2)	124.15(8)	124.09(8)	118.98(10)	112.73(3)	113.24(7)	112.69(6)

[a] Not available.

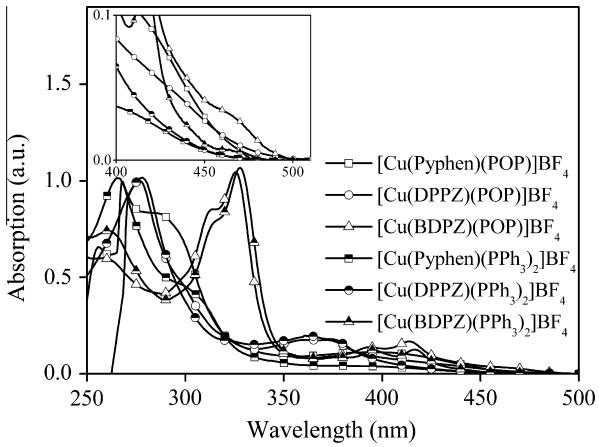

Fig. 2. UV–Vis absorption spectra of Cu(I) complexes in CH_2Cl_2 with a concentration of 1×10^{-5} mol/L. Inset: a magnified view of absorption edges.

similar electronic absorption spectra to corresponding ones of [Cu(N–N)$(PPh_3)_2$]BF_4, it is thus reasonable to expect that the onset electronic transitions of [Cu(N–N)(POP)]BF_4 are MLCT ones as well.

3.3. Photoluminescence (PL) properties

In our previous report, it is found that inter- and inner-molecular π-stacking in solid state Cu(I) complexes can efficiently suppress the geometry relaxation that occurs in excited state, leading to largely enhanced PL performances [24]. Aiming at eliminating potential influences caused by intermolecular π-stacking in solid state, in this paper, all PL parameters are measured using Cu(I) complexes doped poly(methyl methacrylate) (PMMA) films (20 wt%) and summarized in Table 3. As shown in Fig. 3, broad emission spectra are obtained for Pyphen- and DPPZ-based Cu(I) complexes at room temperature, without giving any vibronic progressions. Taking TD-DFT calculations into account, it is thus concluded that the emissive excited states have a MLCT character [20]. What's more, it is observed that enlarged conjugation system in diimine ligand tends to prolong the excited state lifetimes (τ) of [Cu(N–N)$(PPh_3)_2$]BF_4 and [Cu(N–N)(POP)]BF_4 (N–N = Pyphen and DPPZ), compared with those of [Cu(phen)(POP)]BF_4 and [Cu(-phen)$(PPh_3)_2$]BF_4 [13]. However, BDPZ, which owns further enlarged conjugation system, suggests otherwise.

As for [Cu(BDPZ)(POP)]BF_4 and [Cu(BDPZ)$(PPh_3)_2$]BF_4 in both solid state and PMMA films, no emission signal is detected at room temperature, even though there is strong π-stacking in BDPZ-based solid state Cu(I) complexes as we mentioned (see [Cu(BDPZ)$(PPh_3)_2$]BF_4 and [Cu(BDPZ)(POP)]BF_4 CIF files), which has been proved to be efficient on suppressing nonradiative decay process of MLCT excited state [24]. Considering that their onset electronic transition nature is exactly the same with that of [Cu(N–N)$(PPh_3)_2$]BF_4 and [Cu(N–N)(POP)]BF_4 (N–N = Pyphen and DPPZ) as we mentioned, there must be a highly efficient luminescence quencher which suppresses the radiative process of ^{3}MLCT excited state within [Cu(BDPZ)(POP)]BF_4 and [Cu(BDPZ)$(PPh_3)_2$]BF_4.

3.4. Luminescence quencher

Ford and Rodgers develop a strategy to prolong excited state lifetime of d^6-transition metal-polypyridine complexes [26]. In this case an inert hydrocarbon spacer assures that the two tethered chromophores retain their specific properties, where the lowest lying excited state of the pyrene (^{3}LC) lies at a very similar energy to that of the emissive ^{3}MLCT excited state, so that one excited state can be thermally populated from the other at room temperature. This reversible energy transfer strategy has been recently applied to Cu(I) bis(phenanthroline) based complexes aiming at better

Table 2
Calculated percentage composition of frontier molecular orbitals and singlet excitation energy values.

Compound	Character/energy value (eV)		
	HOMO	LUMO	$S_0 \rightarrow S_1$
[Cu(Pyphen)$(PPh_3)_2$]$^+$[a]	Cu(26.4%)PPh_3(68.3%) −7.96	Pyphen(98.8%) −4.77	HOMO → LUMO(79%) 2.65
[Cu(DPPZ)$(PPh_3)_2$]$^+$[a]	Cu(30.2%)PPh_3(62.2%) −7.95	DPPZ(95.1%) −4.83	HOMO → LUMO(98%) 2.64
[Cu(BDPZ)$(PPh_3)_2$]$^+$[a]	Cu(26.8%)PPh_3(62.6%) −7.86	BDPZ(97.2%) −4.92	HOMO → LUMO(95%) 2.48
Pyphen[b]	π/−6.62	π*/−1.97	N/A[c]
DPPZ[b]	π/−6.37	π*/−2.42	N/A[c]
BDPZ[b]	π/−5.73	π*/−2.68	N/A[c]

[a] Calculated with RB3LYP/SBKJC.
[b] Calculated with RB3LYP/6-31G(d).
[c] Not calculated.

Table 3
Summarized photophysical parameters of Cu(I) complexes.

Complexes	λ_{abs} (nm)	λ_{edg} (nm)[a]	λ_{em} (nm)[b]	τ (μs)[c]
[Cu(Pyphen)(PPh3)2]BF4	257 369	474	606	5.4
[Cu(DPPZ)(PPh3)2]BF4	278 361	481	646	6.2
[Cu(BDPZ)(PPh3)2]BF4	328 417	490	603 655[d]	40.6[e]
[Cu(Pyphen)(POP)]BF4	282 398	482	617	6.1
[Cu(DPPZ)(POP)]BF4	277 362	495	620	12.9
[Cu(BDPZ)(POP)]BF4	326 414	500	615 657[d]	70.1[e]
[Cu(Phen)(PPh3)2]BF4[f]	367	N/A[g]	543	8.1
[Cu(Phen)(POP)]BF4[f]	386	N/A[g]	555	4.6

[a] Defined as the wavelength where absorbance ⩽0.001, ±1 nm.
[b] Measured in PMMA films, ±1 nm.
[c] Average lifetimes measured in PMMA films, ±5%, $I = A_1\exp(-t/\tau_1) + A_2\exp(-t/\tau_2)$, $\tau = (A_1\tau_1^2 + A_2\tau_2^2)/(A_1\tau_1 + A_2\tau_2)$.
[d] Measure at 77 K in PMMA films.
[e] Measured for high-energy peak at 77 K in PMMA films.
[f] See Ref. [13].
[g] Not available.

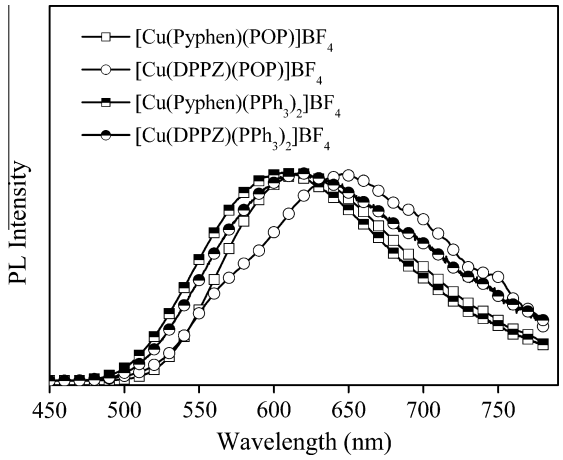

Fig. 3. Emission spectra of 20 wt% Cu(I) complexes in PMMA films with λ_{ex} = 365 nm.

luminescence performances [27]. A schematic presentation of excited state equilibration and electron-configuration transformation is shown in Fig. 4. According to the previous report on Pyphen, DPPZ, and BDPZ, DPPZ owns an optimal triplet state energy similar to that of $[Cu(DPPZ)(P–P)]^+$ emissive ^{3}MLCT excited state, the phenomenon of 'enlarged conjugation system tends to prolong excited state lifetime' as we mentioned becomes reasonable, confirming the correctness of this strategy [25]. However, it is believed that, given the following three conditions, the strategy used to better luminescence performances may compromise or even quench luminescence: A, there is no inert spacer within the ligand, making electron and/or energy transfer between ^{3}LC and ^{3}MLCT excited states more easier to complete; B, the energy level difference between Cu(I) d orbitals and ligand π orbital is small enough for thermal activation, assuring electron-configuration transformation between ^{3}LC and ^{3}MLCT excited states; C, the lowest lying excited state energy of pyrene is smaller than that of ^{3}MLCT, so that the energy transfer between ^{3}LC and ^{3}MLCT excited states becomes partly irreversible.

The three diimine ligands, Pyphen, DPPZ and BDPZ, all own a coplanar conjugation molecular structure, without any inert spacers within their molecules. In addition, density functional theory (DFT) calculations on the three diimine ligands suggest that the increasing number of coplanar phenyl rings dramatically lifts ligand π as shown in Table 2, along with the largely decreased band gap and consequently smaller excited state energy. Given the three conditions being satisfied within BDPZ-based Cu(I) complexes, it is thus reasonable to anticipate that the above mentioned highly efficient luminescence quencher is the ^{3}LC state of BDPZ.

3.5. Quenching mechanism

Based on the above analysis, we propose a potential quenching mechanism as shown in Fig. 5. The ^{3}MLCT excited state originated from intersystem crossing of photoinduced ^{1}MLCT excited state experiences a thermal activated electron-configuration transformation from ^{3}MLCT to ^{3}LC, with the activation energy of E_a. Assuming that ^{3}LC excited state energy is lower than that of ^{3}MLCT excited state, energy transformation between ^{3}MLCT and ^{3}LC thus becomes largely irreversible. Generally, ligand ^{3}LC excited state is dominated by nonradiative decay process at room temperature, correspondingly, leading to luminescence absence of ^{3}MLCT excited state. However, low-temperature may suppress the thermal activated electron-configuration transformation from ^{3}MLCT to ^{3}LC, and depress the nonradiative decay process of ^{3}LC excited state, thus, emissions from ^{3}MLCT and ^{3}LC excited states are expected under low-temperature.

In order to testify the proposed luminescence quenching mechanism, PL spectra are performed on $[Cu(BDPZ)(PPh_3)_2]BF_4$ and $[Cu(BDPZ)(POP)]BF_4$ at 77 K, as well as their diimine ligand, BDPZ. As shown in Fig. 6, both BDPZ-based Cu(I) complexes exhibit two emission peaks at 77 K, centering at 603 and 655 nm for $[Cu(BDPZ)(PPh_3)_2]BF_4$, while 615 and 657 nm for $[Cu(BDPZ)(POP)]BF_4$. Emission peak of the low-energy band seems to be largely immune to phosphorous ligand influence. Comparing with

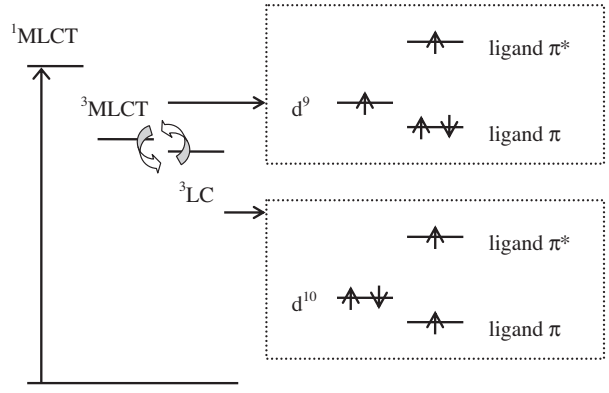

Fig. 4. A schematic presentation of excited state equilibration and electron configuration-transformation in Cu(I) complex.

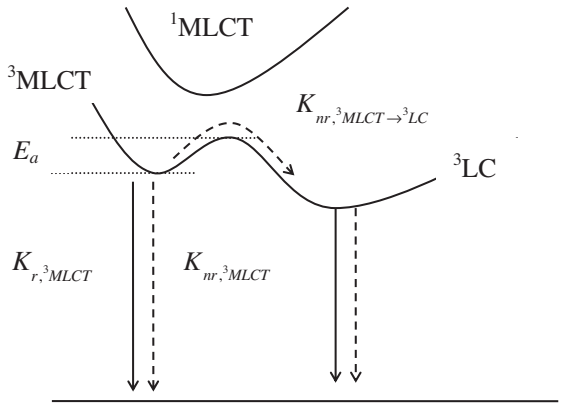

Fig. 5. A schematic presentation of the potential quenching mechanism.

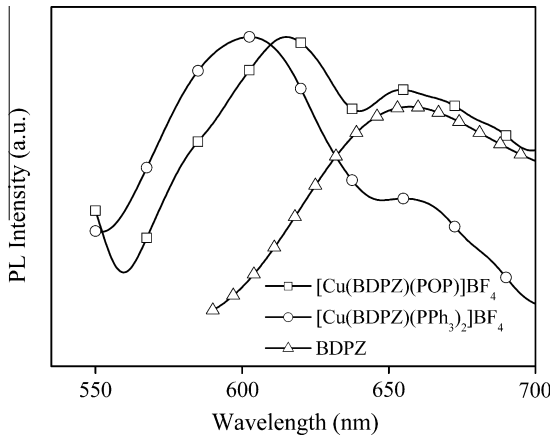

Fig. 6. PL spectra of $[Cu(BDPZ)(PPh_3)_2]BF_4$, $[Cu(BDPZ)(POP)]BF_4$ and BDPZ at 77 K in PMMA films (20 wt%).

low-temperature phosphorescence spectrum of BDPZ peaking at 656 nm, the low-energy emission of $[Cu(BDPZ)(PPh_3)_2]BF_4$ and $[Cu(BDPZ)(POP)]BF_4$ is thus assigned to BDPZ's ^{3}LC excited state emission. On the other hand, phosphorous ligand exerts obvious effect on emission peak of the high-energy band, which is an obvious character of d^{10}-orbitals involved excited state MLCT emission, indicating that the high-energy emission originates from ^{3}MLCT excited state [28]. Thus, herein, the proposed quenching mechanism is first step proved.

3.6. Further analysis on quenching mechanism

Further details are gained from the corresponding decay dynamics recorded at various temperatures from 77 to 137 K. As shown in Fig. 7, the above assigned ^{3}MLCT emission of $[Cu(BDPZ)(PPh_3)_2]BF_4$ red shifts slightly from 603 to 613 nm upon temperature increases from 77 to 137 K, which can be explained as follows. According McMillin's reports on quenching mechanism of d^{10}-orbitals involved emissive MLCT excited state, Cu(I) complexes prefer a tetragonally flattened geometry in excited state, while the tetrahedral-like coordination geometry in ground state. The geometry relaxation that occurs in the excited state facilitates relaxation back to the ground state, as well as reduces the excited state energy, leading to decreased excited state lifetime and emission spectrum red-shift [14,15]. Upon temperature increase, geometry relaxation intensifies, leading to the above mentioned emission spectrum red-shift. Correspondingly, excited state lifetime of the high-energy emission decreases from 40.6 μs at 77 K to 16.5 μs at 137 K, correlating well with geometry relaxation triggered quenching mechanism of d^{10}-orbitals involved MLCT excited state [28]. On the other hand, no obvious emission spectral shift is observed for the low-energy emission. The relative intensity of low-energy emission compared with high-energy emission, however, is largely enhanced upon temperature increases from 77 to 127 K due to the increasing amount of ^{3}LC excited state generated by thermal activation. With an even higher temperature of 137 K, the relative intensity of low-energy emission tends to decrease, suggesting that nonradiative decay process becomes a dominating decay process of ^{3}LC excited state.

With a clear assignment of the two emissions, the overall decay process of $[Cu(BDPZ)(PPh_3)_2]BF_4$ ^{3}MLCT excited state can be described by Eq. (1),

$$K_{obs,^3MLCT} = K_{r,^3MLCT} + K_{nr,^3MLCT} + K_{nr,^3MLCT\rightarrow^3LC} \quad (1)$$

where $K_{obs,^3MLCT}$, $K_{r,^3MLCT}$, $K_{nr,^3MLCT}$, and $K_{nr,^3MLCT\rightarrow^3LC}$ stand for the observed decay rate of ^{3}MLCT excited state, radiative decay rate of ^{3}MLCT excited state, nonradiative decay rate of ^{3}MLCT excited state, and ^{3}MLCT to ^{3}LC nonradiative transformation rate, respectively. As for $K_{r,^3MLCT}$, Lytle and Hercules suggest that the MLCT excited state radiative decay rate remains constant upon various temperatures if there is no phase transformation, suggesting that $K_{r,^3MLCT}$ can be considered as a constant under different temperatures [29]. On the other hand, we mentioned that lower temperature can suppress the ^{3}MLCT excited state nonradiative decay process caused by geometry relaxation, and lead to emission spectrum blue shift. Thus, spectral shift of ^{3}MLCT emission peak can be considered as a pointer presenting $K_{nr,^3MLCT}$ variation under different temperatures. Considering that $[Cu(BDPZ)(PPh_3)_2]BF_4$ ^{3}MLCT emission peak shifts by only 10 nm when temperature increases from 77 to 137 K, it is expected that $K_{nr,^3MLCT}$ variation is also limited within the temperature region of 77–137 K. Thus, it is concluded that $K_{obs,^3MLCT}$ variation upon different temperatures is mainly dominated by that of $K_{nr,^3MLCT\rightarrow^3LC}$. Assuming that the temperature-dependent nonradiative decay rate of ^{3}MLCT excited state is dominated by ^{3}MLCT → ^{3}LC nonradiative process, E_a can be thus derived from the plot of $\ln(K_{obs,^3MLCT})$ versus $\frac{1}{T}$ according to Arrhenius equation.

$$\ln(K_{obs,^3MLCT}) = \ln(A) - \frac{E_a}{RT} \quad (2)$$

The plot of $\ln(K_{obs,^3MLCT})$ versus $\frac{1}{T}$ for ^{3}MLCT emission renders a straight line as shown in Fig. 8, and E_a is calculated to be 5.05 kcal/mol. This energy barrier is small enough for thermal

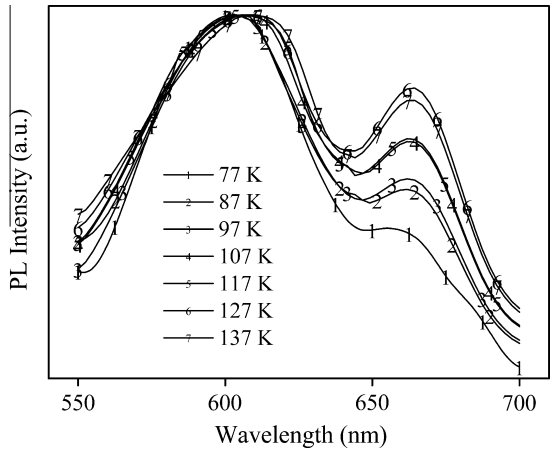

Fig. 7. PL spectra of $[Cu(BDPZ)(PPh_3)_2]BF_4$ at various temperatures from 77 to 137 K in PMMA film (20 wt%).

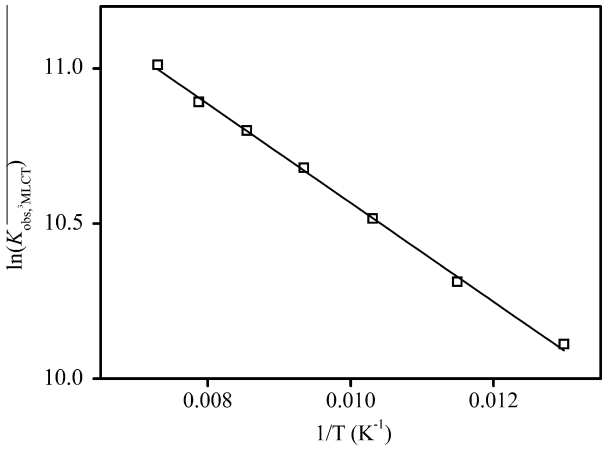

Fig. 8. Plot of $\ln(K_{obs,^3MLCT})$ vs. $\frac{1}{T}$ for $[Cu(BDPZ)(PPh_3)_2]BF_4$ ^{3}MLCT emission.

activation at room temperature, which in turn confirms the possibility of thermal activated electron-configuration transformation from ^{3}MLCT to ^{3}LC. Herein, the quenching mechanism is fully explained and proved.

4. Conclusions

In this paper, we report a series of Cu(I) complexes based on two phosphorous ligands and three diimine ligands. It is found that the introduction of too many fused phenyl rings into diimine ligand leads to ^{3}MLCT emission absence. A detailed analysis suggests that the thermal activated electron-configuration transformation from ^{3}MLCT to ^{3}LC in excited state Cu(I) complex is responsible for the luminescence quenching.

Acknowledgments

The authors gratefully thank the financial supports of the NSFC (Grant Nos. 51172224, 51103145 and 21041007) and the Science and Technology Developing Project of Jilin Province (Grant No. 20100533).

Appendix A. Supplementary material

Supplementary data associated with this article can be found, in the online version, at doi:10.1016/j.ica.2011.12.002.

References

[1] A.P. de Silva, D.B. Fox, T.S. Moody, S.M. Weir, Pure Appl. Chem. 73 (2001) 503.
[2] M. Rudzinski, D.G. Nocera, Mol. Supramol. Photochem. 7 (2001) 1.
[3] M. Elliott, F. Pichot, C.J. Bloom, L.S. Rider, J. Am. Chem. Soc. 120 (1998) 6781.
[4] Y.D. Zhao, A. Richman, C. Storey, N.B. Radford, P. Pantano, Anal. Chem. 71 (1999) 3887.
[5] K.E. Erkkila, D.T. Odom, J.K. Barton, Chem. Rev. 99 (1999) 2777.
[6] L. Prodi, F. Bolletta, M. Montaltri, N. Zaccheroni, Coord. Chem. Rev. 205 (2000) 59.
[7] V. Balzani, A. Juris, M. Venturi, S. Campagna, S. Serroni, Chem. Rev. 96 (1996) 759.
[8] C.A. Bignozzi, R. Argazzi, C.J. Kleverlaan, Chem. Soc. Rev. 29 (2000) 87.
[9] J.V. Balzani, F. Barigelletti, S. Campagna, P. Belser, A. Von Zelewsky, Coord. Chem. Rev. 84 (1988) 85.
[10] D.R. McMillin, K.M. McNett, Chem. Rev. 98 (1998) 1201.
[11] N. Armaroli, Chem. Soc. Rev. 30 (2001) 113.
[12] D.V. Scaltrito, D.W. Thompson, J.A. O'Callaghan, G.J. Meyer, Coord. Chem. Rev. 208 (2000) 243.
[13] Q. Zhang, Q. Zhou, Y. Cheng, L. Wang, D. Ma, X. Jing, F. Wang, Adv. Mater. 16 (2004) 432.
[14] K. Eggleston, D.R. McMillin, K.S. Koenig, A.J. Pallenberg, Inorg. Chem. 36 (1997) 172.
[15] T. Cunningham, K.L.H. Cunningham, J.F. Michalec, D.R. McMillin, Inorg. Chem. 38 (1999) 4388.
[16] R.A. Rader, D. McMillin, M.T. Buckner, T.G. Matthews, D.J. Casadonte, R.K. Lengel, S.B. Whittaker, L.M. Darmon, F.E. Lytle, J. Am. Chem. Soc. 103 (1981) 5906.
[17] P.A. Breddels, M. Berdowski, G. Blasse, J. Chem. Soc. Faraday Trans. 278 (1982) 595.
[18] E.A. Palmer, D.R. McMillin, Inorg. Chem. 26 (1987) 3837.
[19] A. Lavie-Cambot, M. Cantuel, Y. Leydet, G. Jonusauskas, D.M. Bassani, N.D. McClenaghan, Coordin. Chem. Rev. 252 (2008) 2572.
[20] L. Yang, J.K. Feng, A.M. Ren, M. Zhang, Y.G. Ma, X.D. Liu, Eur. J. Inorg. Chem. 10 (2005) 1867.
[21] B. Lei, B. Li, H. Zhang, L. Zhang, W. Li, J. Phys. Chem. C 111 (2007) 11291.
[22] S.M. Kuang, D.G. Cuttell, D.R. McMillin, P.E. Fanwick, R.A. Walton, Inorg. Chem. 41 (2002) 3313.
[23] M. Kranenburg, Y.E.M. van der Brugt, P.C.J. Kamer, P.W.N.M. van Leeuwen, Organometallics 14 (1995) 3081.
[24] L. Zhang, B. Li, Z. Su, Langmuir 25 (2009) 2068.
[25] E.B. Vander Tol, H.J. Van Tamesdonk, J.W. Verhoeven, F.J. Steemers, E.G. Kerver, W. Verboom, D.N. Reinhoudt, Chem. Eur. J. 4 (1998) 2315.
[26] W.E. Ford, M.A.J. Rodgers, J. Phys. Chem. 96 (1992) 2917.
[27] Y. Leydet, D.M. Bassani, G. Jonusauskas, N.D. McClenaghan, J. Am. Chem. Soc. 129 (2007) 8688.
[28] T. McCormick, W.L. Jia, S. Wang, Inorg. Chem. 45 (2006) 147.
[29] F.E. Lytle, D.M. Hercules, J. Am. Chem. Soc. 91 (1969) 253.